Composite Structures 132 (2015) 680–693

Contents lists available at ScienceDirect

Composite Structures

journal homepage: www.elsevier.com/locate/compstruct

Prediction of load–deflection behavior of multi-span FRP and steel reinforced concrete beams

Cengiz Dundar [a,*], Ahmed Kamil Tanrikulu [a], Robert J. Frosch [b]

[a] Civil Engineering Department, Cukurova University, 01330 Adana, Turkey
[b] Lyles School of Civil Engineering, Purdue University, West Lafayette, IN 47907-2051, United States

ARTICLE INFO

Article history:
Available online 10 June 2015

Keywords:
Deflection
Curvature
Effective moment of inertia
FRP reinforcement
Concrete beams
Flexural stiffness

ABSTRACT

This paper presents a numerical procedure to determine the deflection of concrete members reinforced with fiber reinforced polymer (FRP) or steel bars. This procedure is implemented into the stiffness matrix to allow for general use in the structural analysis. It considers effective flexibilities of members in the cracked state using either the curvature distribution along the member or available effective stiffness models under any loading or support condition. In general, structural concrete members can be considered to have three cracked regions (two at the ends and one at midspan) and two uncracked regions along their length. In this numerical procedure, the contributions of these regions to the member stiffness matrix are computed using a numerical integration technique. Using this procedure, a software program is developed which allows for the load–deflection behavior of a member reinforced with either FRP or steel bars and subjected to any loading or support condition to be rapidly determined. This calculation procedure is evaluated using available experimental data on the load–deflection behavior of simple and two-span beams reinforced with FRP and steel bars. Through comparison of the results, it is observed that the load–deflection behaviors calculated using the proposed approach utilizing the member moment–curvature response are consistent with the experimental data. This approach can provide a useful tool for the general calculation of deflection regardless of reinforcement type and can be used throughout the entire range of member behavior up to flexural failure.

1. Introduction

The use of fiber reinforced polymer (FRP) bars in structural concrete has rapidly increased in the last two decades due to their superior durability, excellent corrosion resistance, non-magnetic properties, and high strength-to-weight ratio compared to conventional steel bars. On the other hand, FRP bars have a lower modulus of elasticity compared to steel. Because of this fact, the same amount of reinforcement exhibits larger deflections and crack widths in FRP reinforced concrete members than in steel reinforced concrete members. Hence, the design of such members is typically governed by the serviceability limit state, and accurate determination of deflection becomes very important.

Recently, there has been extensive research to investigate the flexural behavior of FRP reinforced concrete members [1–17]. Many design approaches to calculate the deflection of FRP reinforced concrete members have been proposed in these studies. For the case of service level deflections, some authors have presented additional coefficients taking into account the specific properties of FRP bars. These coefficients are used to modify Branson's equation, which is semi-empirical and commonly used for steel reinforced concrete members in design codes [18], to compute the effective moment of inertia of members reinforced by FRP bars. Others have presented a modified equivalent moment of inertia derived from assumed moment–curvature relationships of the FRP reinforced concrete [19–27]. These models, however, are not completely generalized to work with all loading and support conditions.

The purpose of this research is to develop a numerical procedure that can be implemented into the stiffness matrix in the structural analysis so that the deflection of concrete members reinforced with FRP or steel bars can be determined under any loading or support condition. In this procedure, member flexibility is determined using either the moment–curvature relationship of the reinforced concrete section obtained from a cracked-section analysis or available semi-empirical effective stiffness models. A software program was developed using this procedure which allows the load–deflection behavior of a member reinforced with

* Corresponding author.
E-mail addresses: dundar@cu.edu.tr (C. Dundar), akt@cu.edu.tr (A.K. Tanrikulu), frosch@purdue.edu (R.J. Frosch).

http://dx.doi.org/10.1016/j.compstruct.2015.06.018
0263-8223/

either FRP or steel bars to be rapidly calculated for any loading or support condition.

2. Effective flexibility models for cracked members

To determine the deflection of concrete members reinforced with FRP bars, the effective flexibility of the cracked member is required. In the literature, the effective flexibility of cracked members is calculated using different semi-empirical equations as follows:

ACI 440.1R [28,29]:

$$\frac{1}{E_c I_{eff}} = \frac{1}{E_c I_{cr}}\left[1 - \frac{\omega}{1+\omega}\right] \leqslant \frac{1}{E_c I_g} \quad \text{for } M \geqslant M_{cr} \tag{1}$$

where:

$$\omega = \left(\frac{M_{cr}}{M}\right)^3 \left(\frac{\beta_d I_g}{I_{cr}} - 1\right) \tag{1a}$$

$$\beta_d = \alpha_b\left(\frac{E_f}{E_s} + 1\right); \quad \alpha_b = 0.5 \quad \text{for ACI 440.1R} - 03 \tag{1b}$$

$$\beta_d = 0.2\frac{\rho_f}{\rho_{fb}} \quad \text{for ACI 440.1R} - 06 \tag{1c}$$

where E_c, E_f, and E_s are the modulus of elasticity of concrete, FRP, and steel reinforcement; M is the applied bending moment; M_{cr} is the flexural cracking moment of the section; I_g and I_{cr} are the moments of inertia of the gross and cracked transformed section; and ρ_f and ρ_{fb} are the FRP tensile reinforcement ratio and FRP reinforcement ratio producing balanced strain conditions, respectively.

ACI 440-H [17]:

$$\frac{1}{E_c I_{eff}} = \frac{1}{E_c I_{cr}}\left[1 - \eta\gamma\left(\frac{M_{cr}}{M}\right)^2\right] \leqslant \frac{1}{E_c I_g} \quad \text{for } M \geqslant M_{cr} \tag{2}$$

where:

$$\eta = 1 - \frac{I_{cr}}{I_g}, \quad \gamma = 1.72 - 0.72\left(\frac{M_{cr}}{M}\right) \tag{2a}$$

Bischoff [21], ***ISIS*** [30] ***and CEB*** [31]

$$\frac{1}{E_c I_{eff}} = \frac{1}{E_c I_{cr}}\left[1 - \beta_1\beta_2\left(\frac{M_{cr}}{M}\right)^2\left(1 - \frac{I_{cr}}{I_g}\right)\right] \leqslant \frac{1}{E_c I_g} \quad \text{for } M \geqslant M_{cr} \tag{3}$$

where:

$\beta_1\beta_2 = 1.0$ in Bischoff, $\beta_1\beta_2 = 0.5$ in ISIS and $\beta_1\beta_2 = 0.8$ in CEB models.

Benmokrane et al. [1]

$$\frac{1}{E_c I_{eff}} = \frac{1}{E_c I_{cr}}\left[1 - \frac{(\alpha-1)I_{cr} + \psi}{\alpha I_{cr} + \psi}\right] \leqslant \frac{1}{E_c I_g} \quad \text{for } M \geqslant M_{cr} \tag{4}$$

where:

$$\psi = \left(\frac{M_{cr}}{M}\right)^3\left(\frac{I_g}{\beta} - \alpha I_{cr}\right) \quad \beta = 7; \quad \alpha = 0.84 \tag{4a}$$

Yost et al. [8]:

Same as Eq. (1b) except $\alpha_b = 0.064\left(\frac{\rho_f}{\rho_{fb}}\right) + 0.13$.

Toutanji and Saafi [4]:

$$\frac{1}{E_c I_{eff}} = \frac{1}{E_c I_{cr}}\left[1 - \frac{\left(\frac{M_{cr}}{M}\right)^m\left(\frac{I_g}{I_{cr}} - 1\right)}{1 + \left(\frac{M_{cr}}{M}\right)^m\left(\frac{I_g}{I_{cr}} - 1\right)}\right] \leqslant \frac{1}{E_c I_g} \quad \text{for } M \geqslant M_{cr} \tag{5}$$

where:

$$m = 6 - 10\left(\frac{E_f}{E_s}\right)\rho_f \quad \text{if } \left(\frac{E_f}{E_s}\right)\rho_f < 0.3$$

$$m = 3 \quad \text{if } \left(\frac{E_f}{E_s}\right)\rho_f \geqslant 0.3$$

For all models, the effective flexibility of the member is:

$$\frac{1}{E_c I_{eff}} = \frac{1}{E_c I_g} \quad \text{for } M < M_{cr} \tag{6}$$

The models listed above for calculating the flexibility of a FRP reinforced concrete member are derived from the semi-empirical Branson's equation [32]. In these models, the stress–strain relationships of the concrete and reinforcement are not considered. Instead, empirically derived correction factors are used to improve the deflection prediction of the models.

Other models available in the literature for calculating deflections are based on interpolation between a fully cracked and uncracked state of the member using the curvature distribution. In these models, closed form equations for deflection calculations are developed for only specific member boundary conditions and loading types [19–25].

The present study proposes the use of the complete moment–curvature relationship obtained from a sectional analysis and taking into account the stress–strain relationships of the concrete and reinforcement. A general purpose software program was also developed based on the stiffness matrix formulation of the member in either the cracked or uncracked state.

3. Moment–curvature analysis

Moment–curvature relationships are developed for rectangular concrete sections reinforced with either steel or FRP reinforcement. For this analysis, it is considered that the reinforcement may be in either tension or compression regions. The following material constitutive laws are considered:

3.1. Concrete stress–strain models

Any model for concrete in compression can be used in the analysis procedure. For example, if the CEB-FIB model [33] is used, the following equations are considered:

$$f_c = f'_c\left[\frac{2\varepsilon_c}{\varepsilon_{co}} - \left(\frac{\varepsilon_c}{\varepsilon_{co}}\right)^2\right] \quad \varepsilon_c \leqslant \varepsilon_{co} \tag{7a}$$

$$f_c = f'_c \quad \varepsilon_{co} \leqslant \varepsilon_c \leqslant \varepsilon_{cu} \tag{7b}$$

where f_c and ε_c are the compressive stress and strain in concrete; f'_c is the cylinder compressive strength of concrete; and ε_{co} and ε_{cu} are the strain in concrete at maximum stress and the ultimate strain of concrete as shown in Fig. 1(a) and (b). If the Hognestad model is assumed, only Eq. (7a) is used with the concrete strain $\varepsilon_c \leqslant \varepsilon_{cu}$.

Any model of the tensile stress–strain relationship of concrete can also be used. If a bilinear stress–strain relationship is used, the following equations are considered:

$$f_t = E_c\varepsilon_t \quad \varepsilon_t \leqslant \varepsilon_{cr} \tag{8a}$$

$$f_t = f_r - \frac{f_r}{\varepsilon_{ctu} - \varepsilon_{cr}}(\varepsilon_t - \varepsilon_{cr}), \quad \varepsilon_{ctu} \geqslant \varepsilon_t \geqslant \varepsilon_{cr} \tag{8b}$$

$$\varepsilon_{ctu} = \alpha_{ts}\varepsilon_{cr} \tag{8c}$$

where f_t and ε_t are the tensile stress and strain of the concrete; E_c is the tensile modulus of concrete, assumed to be same as the modulus of elasticity in compression; f_r and ε_{cr} are the modulus of rupture of the concrete and the corresponding cracking strain; and ε_{ctu} is the ultimate tensile strain of the concrete, assumed to be α_{ts} times of the cracking strain (ε_{cr}) as shown in Fig. 1(c). The parameter α_{ts} controls tension stiffening which affects the moment–curvature relationships particularly at initial cracking stages of

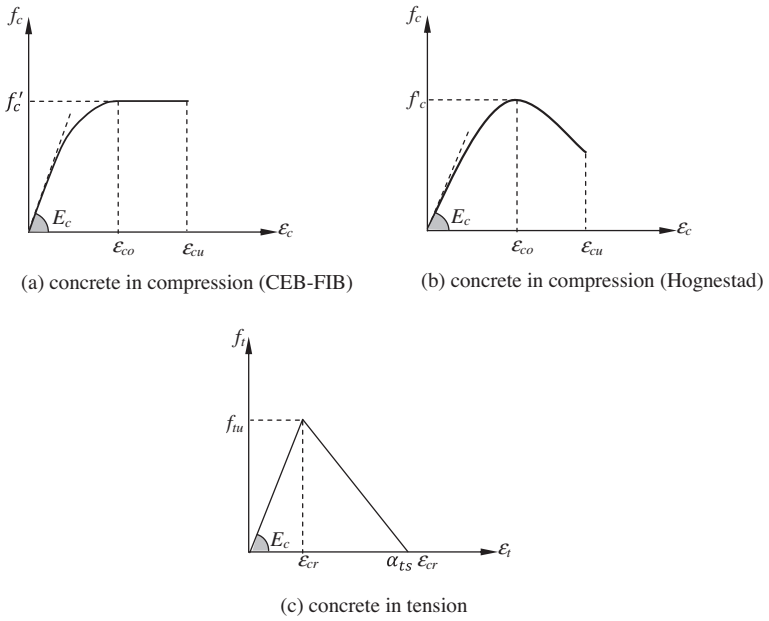

(a) concrete in compression (CEB-FIB) (b) concrete in compression (Hognestad)

(c) concrete in tension

Fig. 1. Concrete stress–strain relationships.

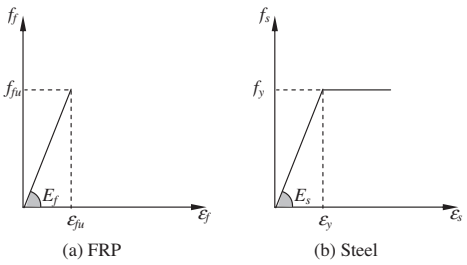

(a) FRP (b) Steel

Fig. 2. Reinforcement bars stress–strain relationships.

the section with lower reinforcement ratios. The values of α_{ts} proposed by different authors [34,35] range from 5 to 25.

3.2. FRP stress–strain model

The stress–strain relationship of FRP bars is linear elastic up to rupture and is given by:

$$f_f = E_f \varepsilon_f \quad \varepsilon_f \leqslant \varepsilon_{fu} \tag{9}$$

where f_f and ε_f are stress and corresponding strain in FRP bars; E_f is the modulus of elasticity of FRP bars; and ε_{fu} is the ultimate strain of FRP bars as shown in Fig. 2(a).

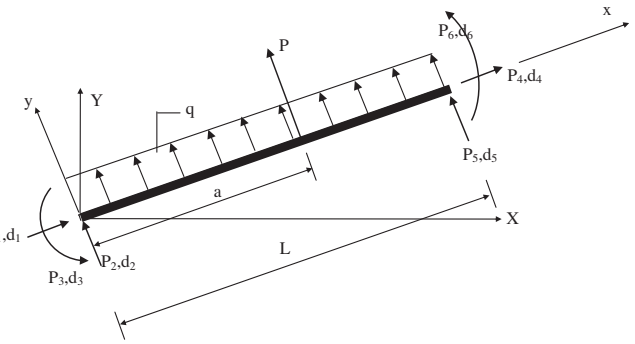

Fig. 4. A typical beam element subjected to span loads.

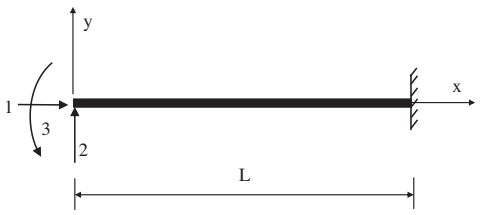

Fig. 5. Cantilever beam model for computing basic nodal deformation parameters.

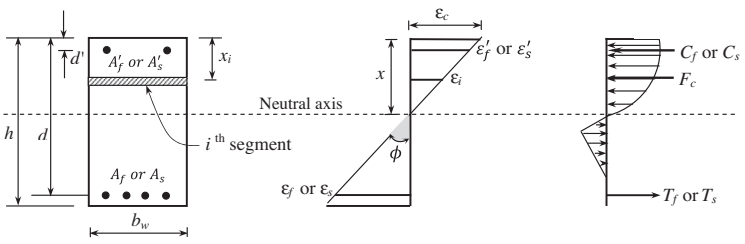

(a) reinforced concrete section (b) strain distribution (c) stress distribution and forces

Fig. 3. Strain, stresses and forces of concrete section reinforced with FRP or steel bars.

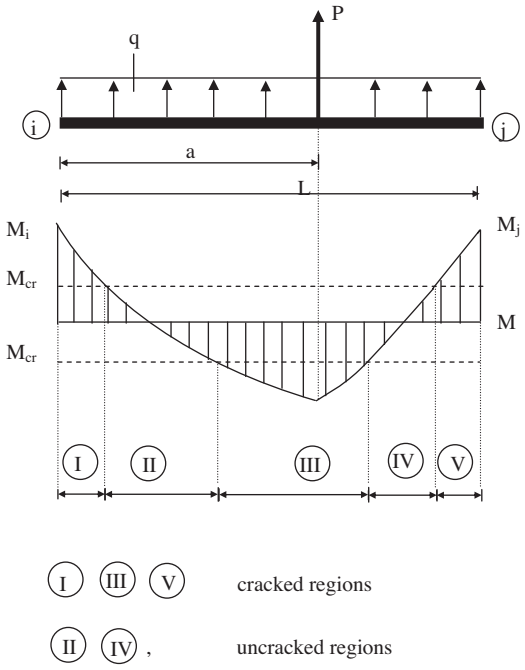

Fig. 6. Cracked and uncracked regions of a span loaded member.

3.3. Steel stress–strain model

The stress–strain relationship of steel is modeled as an elastic–plastic material and is given by:

$$f_s = E_s\varepsilon_s \leqslant f_y \tag{10}$$

where f_s and ε_s are stress and corresponding strain in steel bars; and E_s and f_y are the modulus of elasticity and yield strength of steel as shown in Fig. 2(b).

The moment capacity and curvature equations corresponding to a specific deformation are developed using an incremental deformation technique. Fig. 3 shows a linear distribution of strain, the corresponding stress distribution, and the stress resultants of the FRP or steel reinforced concrete section. The concrete section is divided into n segments. The numerical procedure starts by assuming a small value of strain at the concrete extreme compression fiber. The depth of neutral axis x is initially assumed as half the effective depth of the section and then iteratively corrected until force equilibrium is satisfied. With the assumption that plane sections remain plane after bending, the concrete strain at segment i and strains in the compression and tension reinforcing bars assuming perfect bond between concrete and FRP or steel bars can be expressed as follows:

$$\varepsilon_i = \frac{x - x_i}{x}\varepsilon_c; \quad \varepsilon'_s \text{ or } \varepsilon'_f = \frac{x - d'}{x}\varepsilon_c; \quad \varepsilon_s \text{ or } \varepsilon_f = \frac{x - d}{x}\varepsilon_c \tag{11}$$

where ε_c is the strain at the concrete extreme compression fiber of the section; ε_i is the concrete compressive or tensile strain at mid-depth of the ith segment; ε'_s or ε'_f and ε_s or ε_f are the strains in the compression and tension FRP or steel reinforcement; and d and d' are the bottom and top reinforcement depth, respectively.

From Fig. 3, the following equation can be written considering force equilibrium:

$$\sum F = F_c + (C_f \text{ or } C_s) - (T_f \text{ or } T_s) = 0 \tag{12}$$

where F_c is the resultant concrete force; and $(C_f \text{ or } C_s)$ and $(T_f \text{ or } T_s)$ denote resultant compression and tension in the FRP or steel reinforcement, respectively. Each force is represented as follows:

$$F_c = \sum_{i=1}^{n} f_{ci} h_i b \tag{12a}$$

$$C_f = A'_f E_f \varepsilon'_f \quad C_s = A'_s E_s \varepsilon'_s \tag{12b}$$

$$T_f = A_f E_f \varepsilon_f \quad T_s = A_s E_s \varepsilon_s \tag{12c}$$

For Eq. (12), the initially assumed neutral axis depth is iteratively corrected until sufficient equilibrium accuracy is obtained using the following convergence criterion:

$$\frac{|\sum F|}{|F_c|} \leqslant \epsilon$$

where ϵ is the convergence factor which is taken as 1×10^{-8}.

The curvature and applied moment of the member for a specific concrete extreme compressive strain is then calculated by

$$\phi_M = \frac{\varepsilon_c}{x} \tag{13}$$

$$M = \sum_{i=1}^{n} F_{ci}(x - x_i) + (T_f \text{ or } T_s)(x - d) + (C_f \text{ or } C_s)(x - d') \tag{14}$$

where F_{ci} is the concrete compressive or tensile force at the centroid of the ith segment.

Using this approach, the moment–curvature relationship of the member section is obtained. The flexibility of the member at a specific section is subsequently computed by considering the curvature corresponding with the moment computed from analysis of a structure for given loading and support conditions. The effective flexibility of the member at a specific section can now be written in the same form as the effective flexibility equations given in Section 2 as follows:

$$\frac{1}{E_c I_{eff}} = \frac{1}{E_c I_{cr}}\left[1 - \left(1 - \frac{\phi_M}{M}\right)E_c I_{cr}\right] \leqslant \frac{1}{E_c I_g} \tag{15}$$

Eq. (15) can be used to obtain the stiffness matrix of the member and to compute deflections at any section instead of using the semi-empirical, effective flexibility models given by Eqs. (1)–(6). It should be noted that the applied moment should not exceed the ultimate moment capacity since the ultimate moment capacity is the last point of the moment–curvature curve.

4. Cracked member stiffness matrix

A typical member subjected to a concentrated and uniformly distributed load along with positive end forces with corresponding displacements is shown in Fig. 4. A cantilever model is used (Fig. 5) for computing the relationships between nodal actions and basic deformation parameters of a general planar element. The basic deformation parameters of a general planar element can be established by applying unit loads in order from 1 to 3. The compatibility conditions give the following matrix equation:

$$\begin{bmatrix} d_1 \\ d_2 \\ d_3 \end{bmatrix} = \begin{bmatrix} f_{11} & 0 & 0 \\ 0 & f_{22} & f_{23} \\ 0 & f_{32} & f_{33} \end{bmatrix} \begin{bmatrix} P_1 \\ P_2 \\ P_3 \end{bmatrix} \tag{16}$$

where f_{ij} is the displacement in ith direction due to the application of unit loads in jth direction and can be obtained by using the principal of virtual work as follows:

$$f_{11} = \frac{L}{E_c A} \tag{17a}$$

$$f_{ij} = \int_0^L \frac{M_i M_j}{E_c I_{eff}} dx + \int_0^L \frac{V_i V_j}{\overline{G}_c A} s dx \quad (i,j = 2,3) \tag{17b}$$

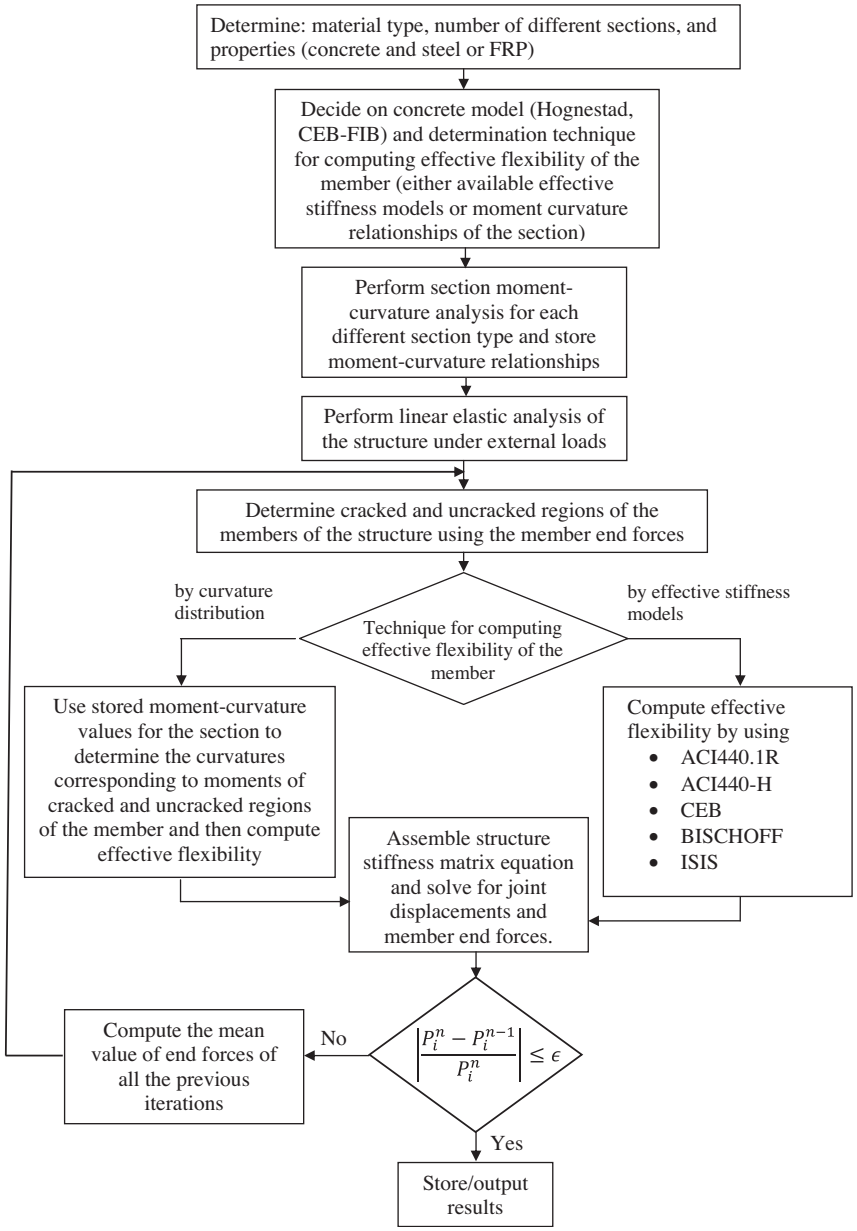

Fig. 7. Flow chart of the proposed algorithm.

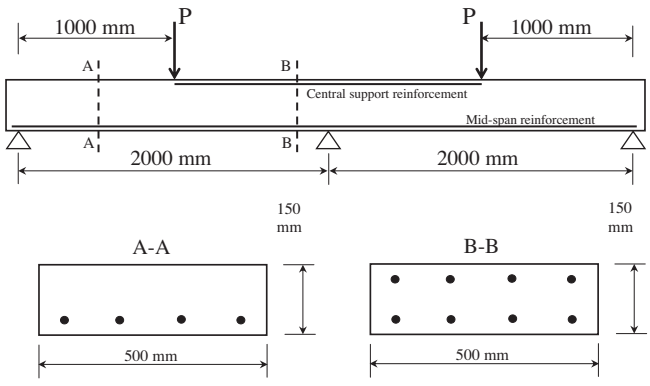

Fig. 8. Continuously supported specimen.

where

$$M_2(x) = x;\ V_2(x) = 1 \tag{18a}$$

$$M_3(x) = -1;\ V_3(x) = 0 \tag{18b}$$

The flexibility coefficients can be evaluated by substituting (M_i, V_i) and (M_j, V_j) into Eq. (17b) as follows:

$$f_{22} = \frac{1}{E_c}\int_0^L \frac{x^2}{I_{eff}}dx + \frac{s}{A}\int_0^L \frac{1}{G_c}dx \tag{19a}$$

$$f_{23} = \frac{1}{E_c}\int_0^L \frac{x}{I_{eff}}dx \tag{19b}$$

$$f_{33} = \frac{1}{E_c}\int_0^L \frac{1}{I_{eff}}dx \tag{19c}$$

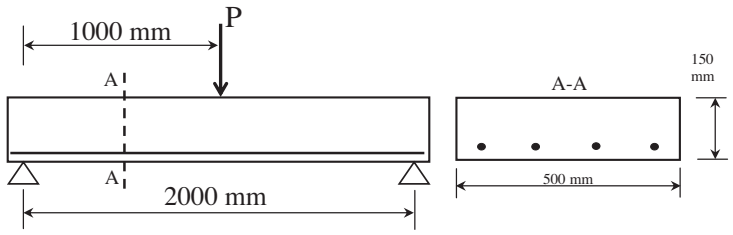

(a) Test Setup a

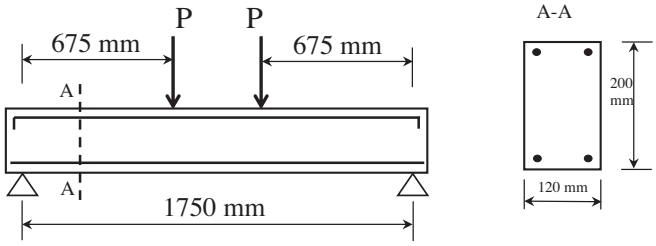

(b) Test Setup b

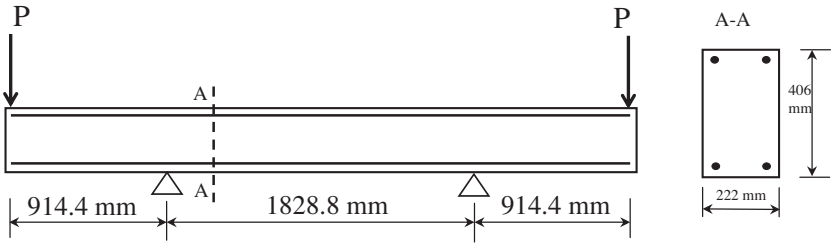

(c) Test setup c

Fig. 9. Simply supported specimens and loading types.

Table 1
Continuously supported specimen details.

Specimen notation	Location	Section A–A			Section B–B			E (GPa)	f'_c (MPa)
		Reinforcement	Material	f_{fu} or f_y (MPa)	Reinforcement	Material	f_{fu} or f_y (MPa)		
C-C-OU[40]	Bottom	5ø12	CFRP	1375	5ø12	CFRP	1375	137	37.8
	Top	–	–	–	3ø8	CFRP	1773		
C-C-UU[40]	Bottom	3ø8	CFRP	1773	3ø8	CFRP	1773	137	42.0
	Top	–	–	–	3ø8	CFRP	1773		
C-C-OO[40]	Bottom	5ø12	CFRP	1375	5ø12	CFRP	1375	137	40.2
	Top	–	–	–	5ø8	CFRP	1773		
C-S_2-UU[40]	Bottom	6ø10	Steel	575	6ø10	Steel	575	200	40.6
	Top	–	–	–	6ø10	Steel	575		
C-B-OU[41]	Bottom	5ø10	BFRP	1350	5ø10	BFRP	1350	50	43.0
	Top	–	–	–	3ø8	BFRP	1250		
C-B-UU[41]	Bottom	3ø8	BFRP	1250	3ø8	BFRP	1250	50	43.0
	Top	–	–	–	3ø8	BFRP	1250		
C-B-OO[41]	Bottom	5ø10	BFRP	1350	5ø10	BFRP	1350	50	42.0
	Top	–	–	–	5ø10	BFRP	1350		
C-S-UU[41]	Bottom	4ø10	Steel	575	4ø10	Steel	575	200	43.0
	Top	–	–	–	4ø10	Steel	575		

In Eq. (17b), (M_i, V_i) and (M_j, V_j) are the bending moments and shear forces due to the application of unit loads in the ith and jth directions; E_c denotes the modulus of elasticity of concrete; A and s are the cross sectional area and shape factor, respectively; and $\overline{G}_c$ is the effective shear modulus of concrete due to cracking. Three different models for $\overline{G}_c$ are as follows:

Al-Mahaidi [36]:

$$\overline{G}_c = \frac{0.4G_c}{\varepsilon_1/\varepsilon_{cr}} \quad \text{for } \varepsilon_1 \geqslant \varepsilon_{cr} \tag{20a}$$

$$\overline{G}_c = G_c \quad \text{for } \varepsilon_1 < \varepsilon_{cr} \tag{20b}$$

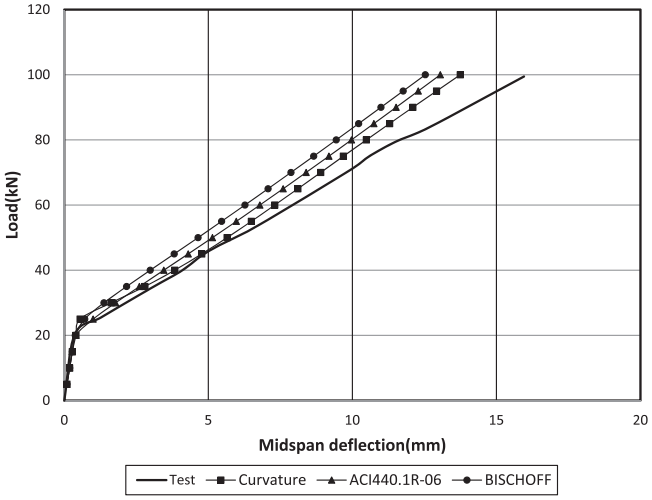

Fig. 10. Experimental and calculated deflections for slab C-C-OU.

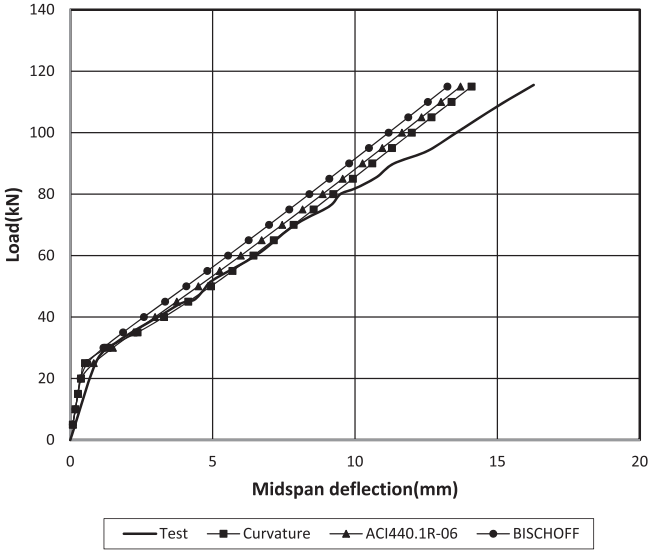

Fig. 11. Experimental and calculated deflections for slab C-C-OO.

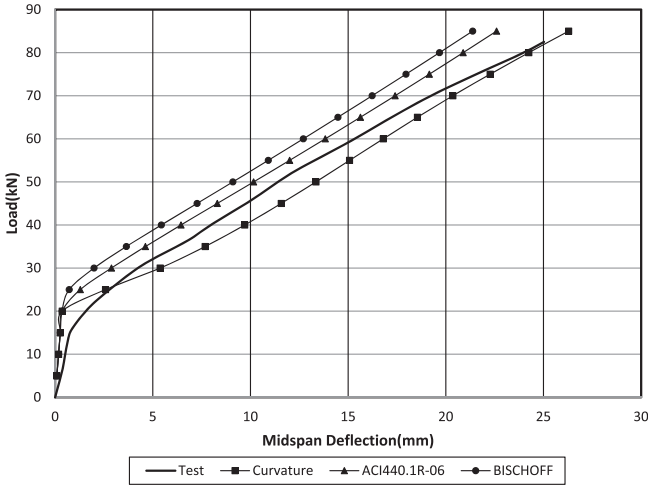

Fig. 12. Experimental and calculated deflections for slab C-C-UU.

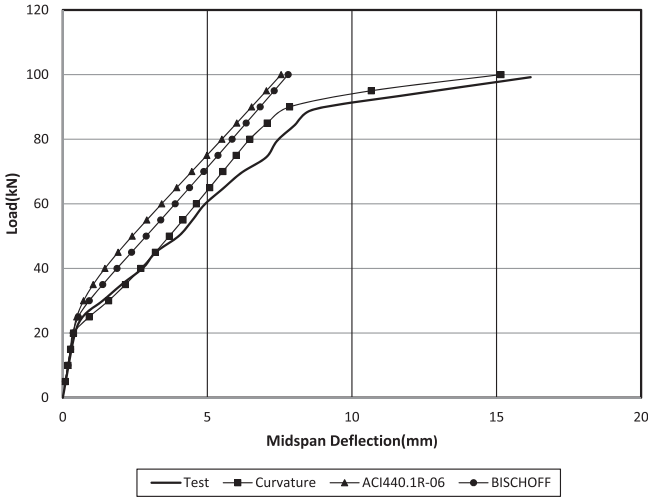

Fig. 13. Experimental and calculated deflections for slab C-S_2-UU.

where G_c is the elastic shear modulus of uncracked concrete; ε_1 is the principal tensile strain normal to the crack; and ε_{cr} is the cracking tensile strain.

Cedolin and Poli [37]:

$$\overline{G}_c = 0.24\, G_c(1 - 250\varepsilon_1) \tag{21}$$

Yuzugullu and Schnobrich [38]:

$$\overline{G}_c = 0.25\, G_c \quad \text{for deep beams} \tag{22a}$$

$$\overline{G}_c = 0.125\, G_c \quad \text{for shear wall and shear wall-frame systems.} \tag{22b}$$

Inverting the flexibility matrix in Eq. (16) and writing the equilibrium equations results in the (6×6) stiffness matrix of the member in the cracked state.

The required displacement in each direction due to the application of span loads can be evaluated by means of the principal of virtual work in the following integral form:

$$f_{10} = 0 \tag{23a}$$

$$f_{i0} = \int_0^L \frac{M_i M_0}{E_c I_{eff}} dx + \int_0^L \frac{V_i V_0}{\overline{G}_c A} s dx \quad (i = 2, 3) \tag{23b}$$

where displacements in the ith direction due to the application of span loads can be evaluated by substituting (M_0, V_0) into Eq. (23b) as follows:

$$M_0(x) = \begin{cases} \frac{qx^2}{2}, & 0 \leqslant x \leqslant a \\ \frac{qx^2}{2}, +P(x-a), & a \leqslant x \leqslant L \end{cases} \tag{24a}$$

$$V_0(x) = \begin{cases} qx, & 0 \leqslant x \leqslant a \\ qx + P, & a < x \leqslant L \end{cases} \tag{24b}$$

$$f_{20} = \frac{q}{2E_c}\int_0^L \frac{x^3}{I_{eff}} dx + \frac{qs}{A}\int_0^a \frac{x}{\overline{G}_c} dx + \frac{P}{E_c}\int_a^L \frac{x(x-a)}{I_{eff}} dx + \frac{s}{A}\int_a^L \frac{(qx+P)}{\overline{G}_c} dx \tag{25a}$$

$$f_{30} = -\frac{q}{2E_c}\int_0^L \frac{x^2}{I_{eff}} dx - \frac{P}{E_c}\int_a^L \frac{(x-a)}{I_{eff}} dx \tag{25b}$$

The fixed end member forces for the case of point and uniformly distributed loads can be evaluated by means of compatibility and equilibrium as follows:

$$P_{10} = P_{40} = 0 \tag{26a}$$

$$P_{20} = -(f_{33} f_{20} - f_{23} f_{30})/(f_{22} f_{33} - f_{23} f_{32}) \tag{26b}$$

$$P_{30} = -(f_{22} f_{30} - f_{23} f_{20})/(f_{22} f_{33} - f_{23} f_{32}) \tag{26c}$$

$$P_{50} = -(q\ L + P + P_{20}) \tag{26d}$$

$$P_{60} = -[-q\ L^2/2 - P(L-a) - P_{20}L + P_{30}] \tag{26e}$$

Finally, the member stiffness equation can be obtained as

$$\underline{k}\ \underline{d} + \underline{P}_0 = \underline{P} \tag{27}$$

where $\underline{k}(6x6)$ is the stiffness matrix, $\underline{d}(6x1)$ is the displacement vector, $\underline{P}_0(6x1)$ is the fixed end force vector, and $\underline{P}(6x1)$ is the total end force vector of the member. Eq. (27) is given in the member oriented coordinate system (x, y); therefore, it should be transformed to the structure oriented coordinate system (X, Y).

The general case of a member with a uniformly distributed and concentrated load is obtained by considering a member having three cracked and two uncracked regions as shown in Fig. 6. In the cracked regions where $M > M_{cr}$, I_{eff} and $\overline{G}_c$ vary with M along the region; therefore, integral operations in Eq. (17) and (23) will be carried out in each region individually using a numerical integration technique which is presented in detail in [39]. The variation of the effective moment of inertia and effective shear modulus of concrete in the cracked regions necessitate the redistribution of moments in the structure. Hence, an iterative procedure is required to obtain the final deflections and internal forces of the structure.

5. Solution algorithm

An algorithm was developed to carry out the numerical calculations to determine the load–deflection behavior of a member before and after cracking using either the moment–curvature relationships of the steel or FRP reinforced members or available empirical effective stiffness models. The following are considered in the numerical procedure:

(a) The member has a rectangular cross section reinforced with either FRP or steel bars in tension and compression zones.
(b) Any concrete stress–strain model can be used for the compression and tension zones.
(c) An elastic–plastic stress–strain model for steel or a linear elastic stress–strain model for FRP is used in both tension and compression.
(d) Moment–curvature relationships of the section or any available effective stiffness model considering tension stiffening can be used for computing the member stiffness in the cracked state.
(e) The structure under consideration can have single or multi-span beams, and the spans may be subject to a uniformly distributed as well as a concentrated load. If the member has more than one concentrated load, additional nodes are introduced under the concentrated loads. Furthermore, additional nodes are introduced where deflection calculations are required.
(f) Concentrated loads may be incrementally increased up to a desired load limit.
(g) The members are divided into two uncracked and three cracked regions to provide a general solution, and the contribution of each region to member stiffness is computed using a numerical integration technique.
(h) For each different reinforced section in the structure, the moment–curvature relationship is obtained up to the ultimate moment capacity of the section. The numerical

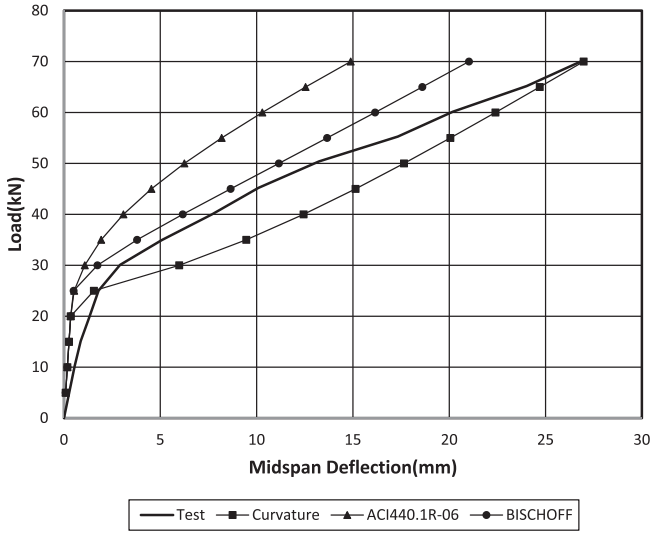

Fig. 14. Experimental and calculated deflections for slab C-B-OU.

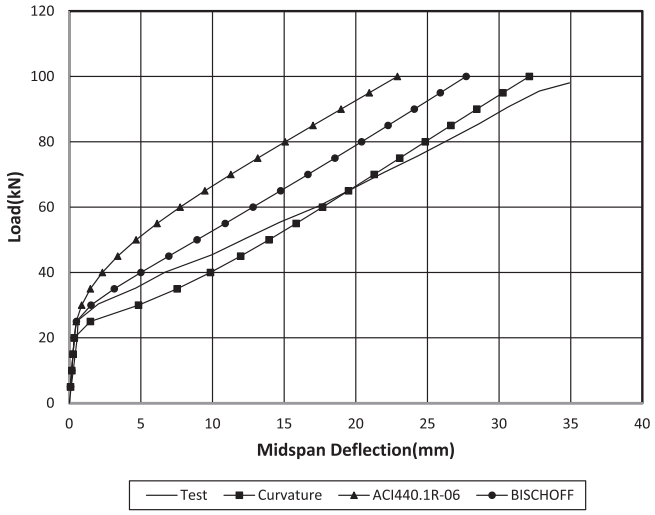

Fig. 15. Experimental and calculated deflections for slab C-B-OO.

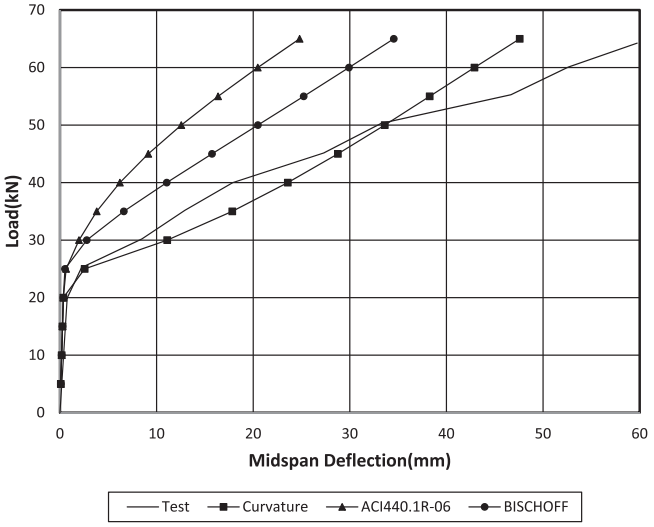

Fig. 16. Experimental and calculated deflections for slab C-B-UU.

procedure starts (after selecting the material type, section parameters, and concrete model) by assuming an initial value for the strain (ε_c) in the concrete at the extreme compression fiber and a location for the neutral axis. Iterations are performed until strain compatibility and equilibrium are satisfied. The values of moment and curvature for the assumed concrete strain are then determined. By incrementing ε_c, a new moment and curvature are computed. Corresponding moment–curvature values are continued to be generated until the maximum specified value for the extreme compression fiber of the concrete strain, ε_{cu} is reached.

With this calculation procedure, a software program was developed. Joint displacements and member end forces are obtained using an iterative procedure as illustrated in the flow chart provided in Fig. 7. The member end forces used at each iteration are taken as the mean value of the end forces of all previous iterations.

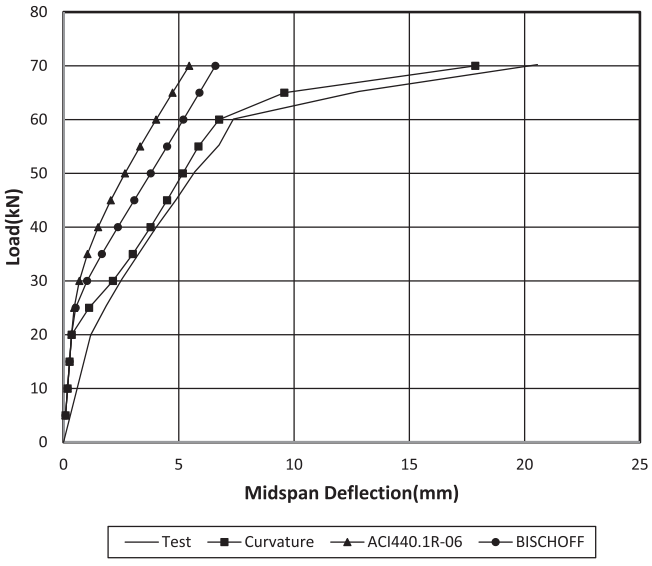

Fig. 17. Experimental and calculated deflections for slab C-S-UU.

This procedure accelerates convergence of the algorithm. The following convergence criterion is used:

$$\left|\frac{P_i^n - P_i^{n-1}}{P_i^n}\right| \leqslant \epsilon \tag{25}$$

where ϵ is the convergence factor which is taken as 1×10^{-2}, n is the iteration number, and P_i^n $(i = 1 - 6)$ is the end forces of each member of the structure for the nth iteration.

6. Evaluation of the proposed procedure

To evaluate the accuracy of the calculation procedure, the calculated results are compared with the load–deflection response from several studies. These studies include the following:

(a) Three continuous and two simply supported concrete slabs reinforced with carbon fiber polymer (CFRP) bars, three continuously and two simply supported concrete slabs reinforced with basalt fiber polymer (BFRP) bars, and two continuously supported concrete slabs reinforced with steel bars tested by Mahroug et al. [40,41]
(b) Two simply supported concrete beams reinforced with glass fiber polymer (GFRP) bars tested by Rafi and Nadjai [42]
(c) Three simply supported concrete beams with overhangs reinforced with glass fiber polymer GFRP, aramid fiber polymer (AFRP), and steel bars tested by Mosley et al. [43].

The test setups for these studies are illustrated in Figs. 8 and 9, and the specimens were analyzed based on the given support and loading conditions. Load–deflection curves of the specimens were calculated using the moment–curvature relationships of the steel or FRP reinforced concrete sections as well as the ACI 440.1R-06 and Bischoff's semi-empirical effective stiffness model equations. These models were selected for comparison because the ACI 440.1R-06 expression represents a weighted average of the uncracked (E_cI_g) and cracked (E_cI_{cr}) flexural stiffness of the member and is widely used for FRP reinforced members whereas Bischoff's expression represents a weighted average flexibility ($1/EI$) of the member which is considered more accurate for lightly

Table 2
Simply supported specimen details.

Specimen notation	Loading type	Location	Reinforcement	Material	f_{fu} or f_y (MPa)	E (GPa)	f'_c (MPa)
S-C-O[40]	(a)	Bottom Top	5∅12 –	CFRP –	1375 –	137 –	43.0
S-C-U[40]	(a)	Bottom Top	3∅8 –	CFRP –	1773 –	137 –	43.4
S-B-O[41]	(a)	Bottom Top	5∅10 –	BFRP –	1350 –	50 –	44.0
S-B-U[41]	(a)	Bottom Top	3∅8 –	BFRP –	1250 –	50 –	41.0
BRC1[42]	(b)	Bottom Top	2∅9.5 2∅8	CFRP Steel	1676 566	234 194	43.0
BRC2[42]	(b)	Bottom Top	2∅9.5 2∅8	CFRP Steel	1676 566	234 194	42.0
B-G1-1[43]	(c)	Bottom Top	2∅10 3∅16	Steel GFRP	524 607	200 40.5	38.6
B-A-1[43]	(c)	Bottom Top	2∅10 3∅16	Steel AFRP	524 1420	200 47.1	39.2
B-S-1[43]	(c)	Bottom Top	2∅10 3∅16	Steel Steel	524 524	200 200	38.1

reinforced members. To compute the tensile strength and modulus of elasticity of concrete, the following equations were used.

$$f_r = 0.62\sqrt{f'_c} \quad \text{(MPa)} \tag{26a}$$

$$E_c = 4733\sqrt{f'_c} \quad \text{(MPa)} \tag{26b}$$

In the analysis, the CEB-FIB model was used for concrete stress–strain ($\varepsilon_{co} = 0.002$ and $\varepsilon_{cu} = 0.0035$) relationship in compression, the tension-stiffening parameter (α_{ts}) was set to 5 for the concrete stress–strain relationship in tension, and Al-Mahaidi model was used for the effective shear modulus of concrete due to cracking. It should be noted that the tension stiffening parameter (α_{ts}) was varied from 2 to 10 to evaluate the influence of this parameter. It was determined based on comparison with the experimental load–deflection curves that the best results were obtained when this parameter was set to 5. Consequently, a constant value of 5 was used for all analyses.

6.1. Continuously supported slab specimens

Two groups of two span continuously supported slab specimens were evaluated, and the test setup is shown in Fig. 8. The first group consists of C-C-OU, C-C-UU, and C-C-OO reinforced with CFRP bars and C-S_2-UU reinforced with steel bars [40]. The second group consists of C-B-OU, C-B-UU, and C-B-OO reinforced with BFRP bars and C-S-UU reinforced with steel bars [41]. Geometric and material properties for these specimens are given in Table 1.

Figs. 10–17 present the measured and calculated midspan load–deflection curves of these specimens. There is generally good agreement between the analytical and experimental curves. The experimental curves, however, are slightly softer because they represent localized responses that depend on the proximity to a primary crack and potentially also include the effects of moment redistribution whereas the analytical curves represent homogenized load–deflection responses.

The midspan load–deflection curves for Specimens C-C-OU, C-C-OO, C-C-UU and C-S_2-UU are shown in Figs. 10–13. As seen, the load–deflection curves obtained using moment–curvature are closer to the experimental curves for Specimens C-C-UU and C-S_2-UU than the ACI 440.1R-06 and Bischoff's effective stiffness equations which provide a stiffer response. For Specimens C-C-OU and C-C-OO, the load–deflection curves obtained using moment–curvature and the ACI 440.1R-06 and Bischoff's effective stiffness equations are in good agreement with the experimental curves until approximately 70% of the ultimate load. Beyond this

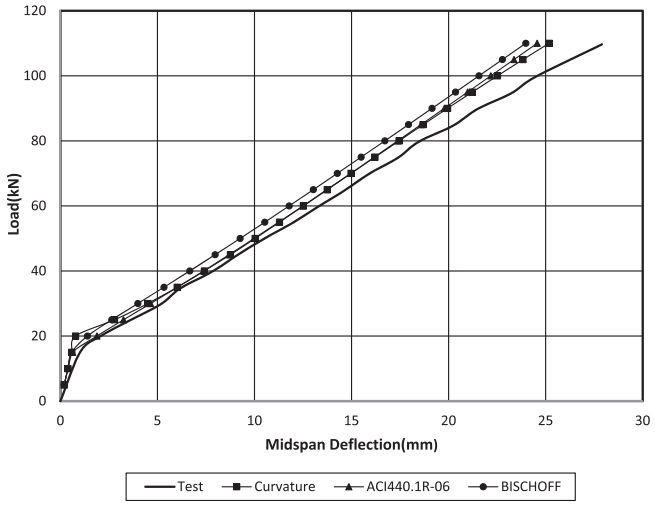

Fig. 18. Experimental and calculated deflections for slab S-C-O.

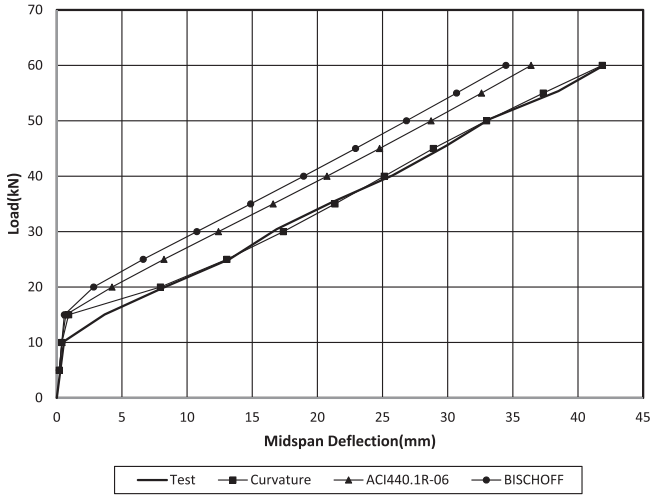

Fig. 19. Experimental and calculated deflections for slab S-C-U.

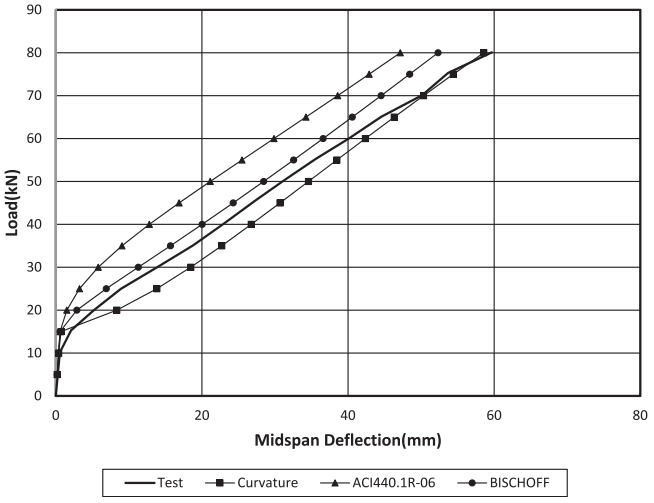

Fig. 20. Experimental and calculated deflections for slab S-B-O.

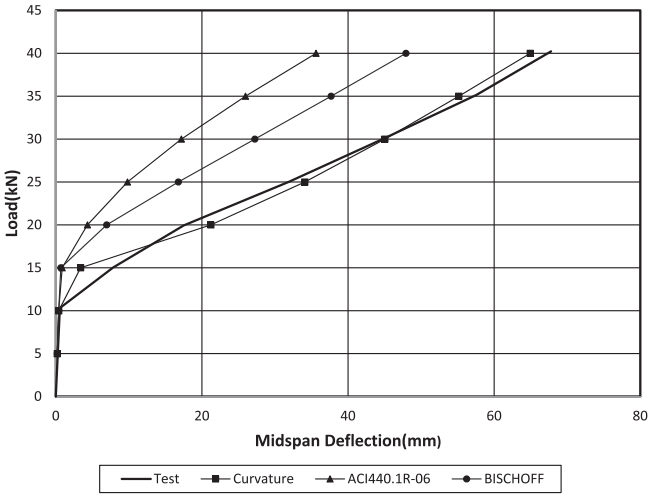

Fig. 21. Experimental and calculated deflections for slab S-B-U.

point, the predicted load–deflection curves provide a slightly stiffer response with respect to the experimental. The difference between the experimental and calculated values may be attributed to the assumption that bonding between the reinforcement and concrete is perfect. In reality, some bond slippage in CFRP bars may take place during testing at these higher loads.

For Specimens C-B-OU, C-B-OO, C-B-UU and C-S-UU, the load–deflection curves (Figs. 14–17) obtained using the moment–curvature relationship show significantly better agreement than the load–deflection curves obtained using the ACI 440.1R-06 and Bischoff's effective stiffness equations which again result in a stiffer response. Furthermore, as evident in Fig. 17, the ACI 440.1R-06 and Bischoff's expressions are not appropriate if post-yielding response is required. This was also observed in Fig. 13.

One of the differences in the two series of tests is the stiffness of the reinforcement. Basalt fiber bars have a stiffness that is approximately 1/3 of the carbon fiber bars. This reduced axial stiffness of the reinforcement clearly has a detrimental influence on the calculation accuracy of the ACI 440.1R-06 model.

6.2. Simply supported slab/beam specimens

Three groups of simply supported specimens were evaluated, and the test setups are shown in Fig. 9. The first group of simply supported slabs subjected to three point bending consists of S-C-O and S-C-U reinforced with CFRP bars as well as S-B-O and S-B-U reinforced with BFRP bars [41]. The second group of simply supported beams subjected to four point bending consists of BRC1 and BRC2 reinforced with CFRP bars in tension and steel bars in compression [42]. The third group of simply supported beams with cantilevers on both sides and point loaded at the ends consists of B-A-1 reinforced with AFRP bars, B-G1-1 reinforced with GFRP bars, and B-S-1 reinforced with steel bars in tension, and all were reinforced with steel bars in compression [43]. Geometric and material properties for these specimens are given in Table 2.

Figs. 18–21 present the experimental and calculated midspan load–deflection curves using the moment–curvature relationship as well as the ACI 440.1R-06 and Bischoff's semi-empirical effective stiffness equations for slabs S-C-O, S-C-U, S-B-O and S-B-U. All of the load–deflection curves using moment–curvature show excellent agreement with the experimental curves whereas the curves predicted using the ACI 440.1R-06 and Bischoff models provide a stiffer response for Slabs S-C-U and S-B-U. In evaluating these curves further, it is seen that for the carbon reinforced specimens, the ACI 440 and Bischoff's expressions corresponded well for S-C-O, but not quite as well for S-C-U. The primary difference in these specimens was that S-C-U had a significantly lower amount of flexural reinforcement. Similarly for the basalt specimens (S-B-O vs S-B-U), a reduction of the area of reinforcement resulted in the ACI 440 expression greatly over estimating the stiffness. A

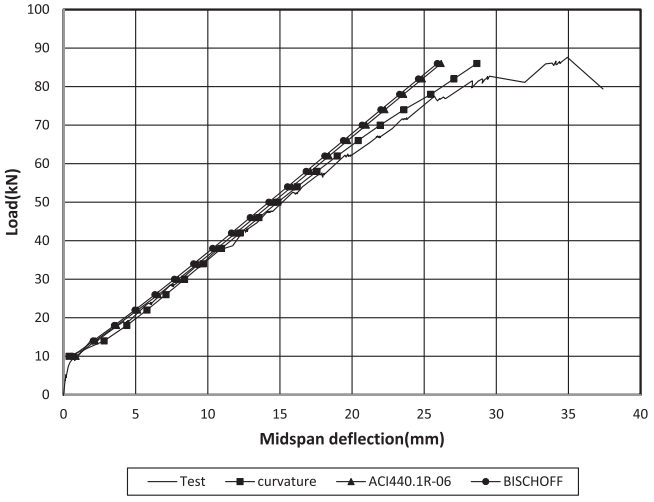

Fig. 22. Experimental and calculated deflections for beam BRC1.

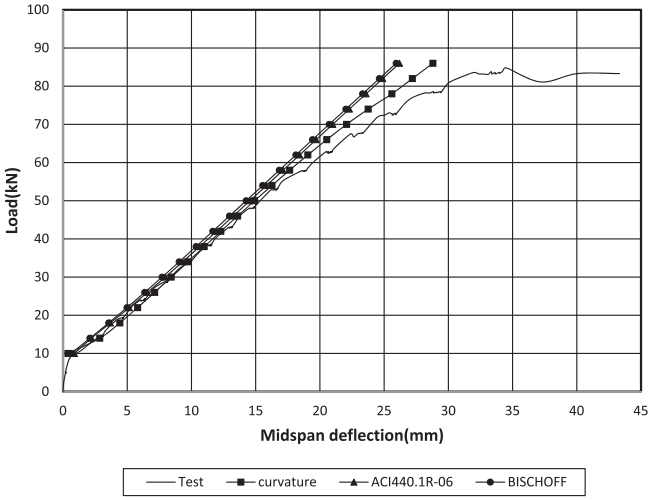

Fig. 23. Experimental and calculated deflections for beam BRC2.

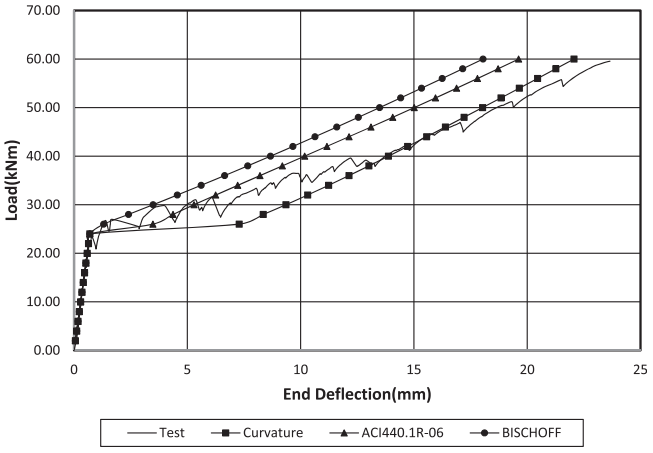

(a) End deflection

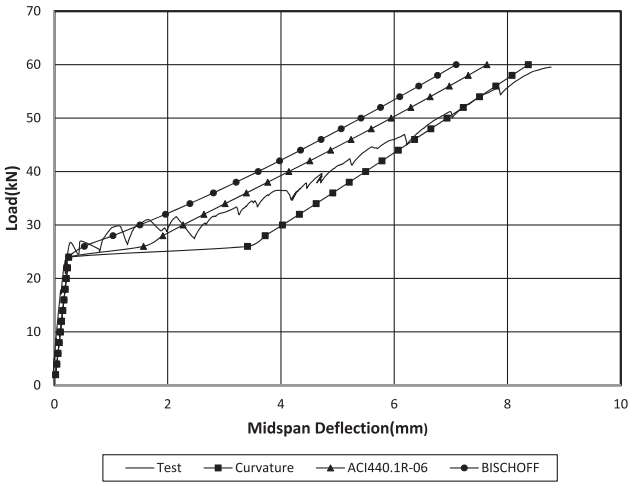

(b) Midspan deflection

Fig. 24. Experimental and calculated deflections for beam B-G1-1.

similar trend, but not as significant, is observed with the Bischoff expression. Finally, in comparing specimens S-C-U and S-B-U which contained the same amount of reinforcement, but different axial stiffnesses of the reinforcement, it is evident that the flexural stiffness of the member is impacting the results of the ACI 440 model. The moment–curvature approach, however, is capable of providing consistent predictions regardless of the flexural stiffness.

Figs. 22 and 23 present the experimental and calculated midspan load–deflection curves for beams BRC1 and BRC2. There is very good agreement between the experimental and predicted curves for all models. The ACI 440.1R-06 and Bischoff models result in a slightly stiffer responses for both beams as failure was approached.

The third group of specimens were designed to evaluate the bond strength of the FRP bars [43]. Therefore, the specimens were reinforced for negative moment with three 16 mm bars in the top of the specimens and were lap spliced at the center of the constant moment region. Two 9.53 mm steel bars were included at the bottom of the specimens. Specimens B-G1-1, B-A-1 and B-S-1 all had a 457 mm splice length, and Figs. 24–26 present the experimental and calculated load–deflection curves for both the cantilever and at midspan of the specimen.

Fig. 24 presents the end and midspan load–deflection curves for glass specimen B-G1-1. As shown, the experimental and calculated curves obtained using moment curvature are in good agreement for both the end and midspan deflections whereas the ACI 440.1R-06 and Bischoff effective stiffness models provide a stiffer response at both locations, especially for the end deflection.

Fig. 25 presents the end and midspan load–deflection curves for aramid specimen B-A-1. The deflections calculated at the end of the beam using moment curvature show excellent agreement with the experimental results whereas the ACI 440.1R-06 model results in a significantly stiffer response. On the other hand, the midspan load–deflection calculated with the moment–curvature relationship provided a slightly softer behavior with respect to the experimental. This difference may be due to the lap-spliced region at midspan because the top reinforcement is doubled in this region. The ACI 440.1R-06 model again provides a significantly stiffer response. The Bischoff model also provides a stiffer response with respect to the experimental behavior but a softer response compare to that of ACI 440.

Fig. 26 presents the end and midspan load–deflection curves for the steel specimen B-S-1. As shown, there is good agreement between the experimental values and those calculated using

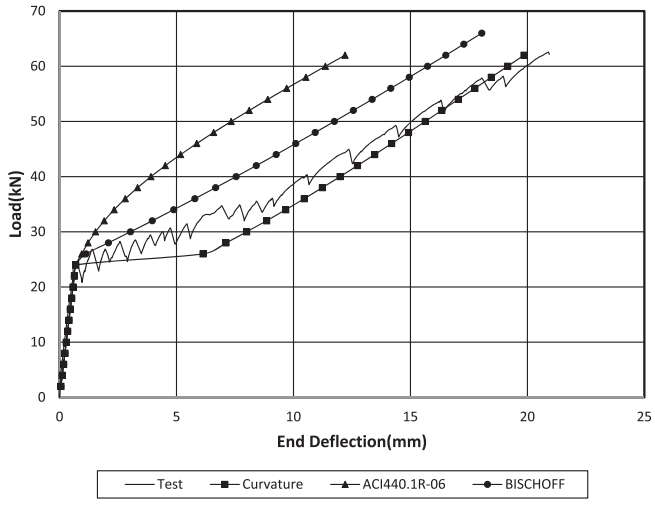

(a) End deflection

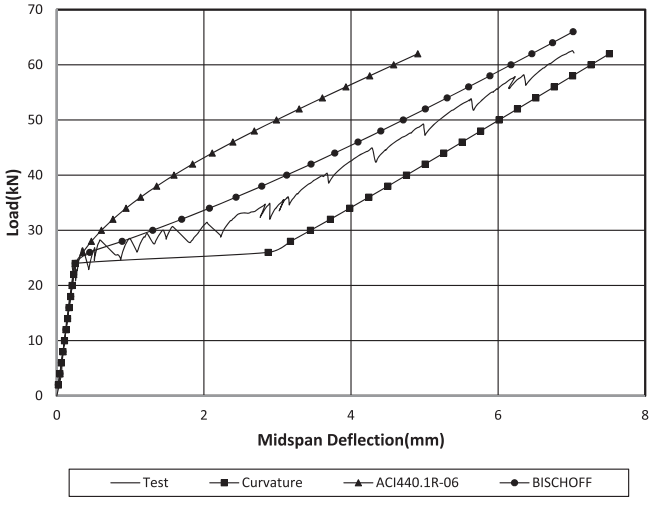

(b) Midspan deflection

Fig. 25. Experimental and calculated deflections for beam B-A-1.

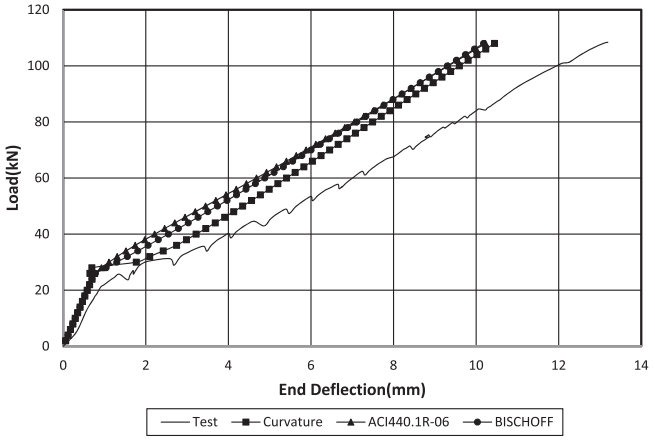

(a) End deflection

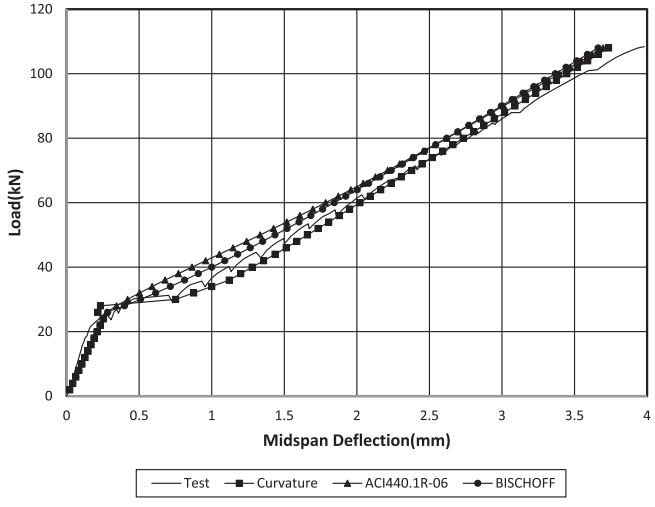

(b) Midspan deflection

Fig. 26. Experimental and calculated deflections for beam B-S-1.

moment curvature as well as the ACI 440.1R-06 and Bischoff models for midspan deflection. On the other hand, a slightly stiffer response is obtained for the end point deflection with respect to the experimental for all approaches.

7. Summary and conclusions

A numerical procedure was developed for calculating the deflection of concrete members reinforced with either fiber-reinforced polymer (FRP) or steel bars. This procedure considers the effective flexibilities of cracked members using either the curvature distribution along the member or available semi-empirical effective stiffness models. With this procedure, statically indeterminate structures, such as continuously supported beams subjected to any intermediate loading, can be analyzed. Furthermore, the load–deflection behavior of a concrete member reinforced with either FRP or steel bars can be rapidly determined using this approach.

The numerical procedure was used to calculate the deflections of 17 short-term flexural tests of FRP and steel reinforced concrete beams and slabs reported in the literature. To evaluate the validity of the proposed procedure, comparisons are made between the experimental and analytical load–deflection response of the 17 reinforced concrete specimens. The results of this study demonstrate considerable promise in accurately calculating the load–deflection behavior of reinforced concrete specimens. The calculated load–deflection curves, which use the moment–curvature relationship, in general provided excellent agreement with the experimental curves. On the other hand, the ACI 440.1R-06 semi-empirical effective stiffness model provides a varied response. In general, a stiffer response is provided as the flexural stiffness is decreased which is common with the use of low modulus reinforcement materials or low flexural reinforcement ratios. On the other hand, the Bischoff model provides a softer response than the ACI 440 model for the aforementioned case because it represents a weighted average of flexibility which is more appropriate for modeling deflections over a wider range of member stiffness [25].

Using this analysis procedure and integrating the moment–curvature response provides a number of benefits. First, the analysis can account for varied reinforcement materials from low stiffness FRP materials such as glass to steel. Second, the analysis inherently accounts for the variations in the flexural reinforcement ratio. Finally, the analysis can calculate deflections across the entire range of behavior from uncracked up to flexural failure including post-yielding response if applicable. Therefore, this procedure is not limited to a range of behavior such as only for serviceability deflections. Overall, the approach provides a general deflection calculation procedure.

Acknowledgements

Financial support for this investigation was provided by the Higher Education Council (YOK) of Turkey which enabled part of this work to be conducted at the Bowen Laboratory of Purdue University, West Lafayette, Indiana. The support of both institutions is gratefully acknowledged. A software program written in FORTRAN and in Excel with Visual Basic codes was developed using the procedure outlined in this paper. The software can be obtained free of charge from the authors upon request.

References

[1] Benmokrane B, Chaallal O, Masmoudi R. Flexural response of concrete beams reinforced with FRP reinforcing bars. ACI Struct J 1995;91(2):46–55.
[2] Masmoudi R, Theriault M, Benmokrane B. Flexural behavior of concrete beams reinforced with deformed fiber reinforced plastic reinforcing rods. ACI Struct J 1998;95(6):665–75.
[3] Alsayed SH. Flexural behavior of concrete beams reinforced with GFRP bars. Cem Concr Compos 1998;20:1–11.
[4] Toutanji HA, Saafi M. Flexural behavior of concrete beams reinforced with glass fiber-reinforced polimer (GFRP) bars. ACI Struct J 2000;97(5):712–9.
[5] Abdalla HA. Evaluation of deflection in concrete members reinforced with fibre reinforced polymer (FRP) bars. Compos Struct 2002;56:63–71.
[6] Thiagarajan G. Experimental and analytical behavior of carbon fiber-based rods as flexural reinforcement. J Compos Constr 2003;7(1):64–72.
[7] Toutanji H, Deng Y. Deflection and crack-width prediction of concrete beams reinforced with glass FRP rods. Constr Build Mater 2003;17:69–74.
[8] Yost JR, Gross SP, Dinehart DW. Effective moment of inertia for glass fiber-reinforced concrete beams. ACI Struct J 2003;100(6):732–9.
[9] Rashid MA, Mansur MA, Paramasivam P. Behavior of aramid fiber-reinforced polymer reinforced high strength concrete beams under bending. J Compos Constr 2005;9(2):117–27.
[10] Ashour AF. Flexural and shear capacities of concrete beams reinforced with GFRP bars. Constr Build Mater 2006;20:1005–15.
[11] Nayal R, Rasheed HA. Tension stiffening model for concrete beams reinforced with steel and FRP bars. J Mater Civil Eng 2006;18(6):831–41.
[12] Kara IF, Ashour AF. Flexural performance of FRP reinforced concrete beams. Compos Struct 2012;94:1616–25.
[13] Kassem C, Farghaly AS, Benmokrane B. Evaluation of flexural behavior and serviceability performance of concrete beams reinforced with FRP bars. J Compos Constr 2011;15(5):682–95.
[14] Al-Sunna R, Pilakoutas K, Hajirasouliha I, Guadagnini M. Deflection behavior of FRP reinforced concrete beams and slabs: an experimental investigation. Compos: Part B 2012;43:2125–34.
[15] Kara IF, Ashour AF. Moment distribution in continuous FRP reinforced concrete beams. Constr Build Mater 2013;49:939–48.
[16] Barris C, Torres L, Comas J, Mias C. Cracking and deflections in GFRP RC beams: an experimental study. Compos: Part B 2013;55:580–90.
[17] El-Nemr A, Ahmed EA, Benmokrane B. Flexural behavior and serviceability of normal-and high-strength concrete beams reinforced with glass fiber-reinforced polymer bars. ACI Struct J 2013;110(6):1077–88.
[18] American Concrete Institute (ACI). Building code requirement for structural concrete, Standard 318-11, ACI, Farmington Hills, Mich; 2011.
[19] Razaqpur AG, Svecova D, Cheung S. Rational method for calculating deflection of fiber-reinforced polymer reinforced beams. ACI Struct J 2000;97(1):175–83.
[20] Rasheed HA, Nayal R, Melhem H. Response prediction of concrete beams reinforced with FRP bars. Compos Struct 2004;65:193–204.
[21] Bischoff PH. Reevaluation for deflection prediction for concrete beams reinforced with steel and fiber reinforced polymer bars. J Struct Eng 2005;131(5):752–67.
[22] Bischoff PH. Deflection calculation of FRP reinforced concrete beams based on the modifications to the existing Branson equation. J Compos Constr 2007;11(1):4–14.
[23] Bischoff PH, Gross SG. Equivalent moment of inertia based on integration of curvature. J Compos Constr 2011;15(3):263–73.
[24] Bischoff PH, Gross SG. Design approach for calculating deflection of FRP-reinforced concrete. J Compos Constr 2011;15(4):490–9.
[25] Bischoff PH, Scanion A. Effective moment of inertia for calculating deflections of members containing steel reinforcement and fiber-reinforced polymer reinforcement. J Struct Eng 2007;104(1):68–75.
[26] Mota C, Alminar S, Svecova D. Critical review of deflection formulas for FRP-RC members. J Compos Constr 2006;10(3):183–94.
[27] Kara IF, Ashour AF, Dundar C. Deflection of concrete structures reinforced with FRP bars. Compos: Part B 2013;44:375–84.
[28] ACI Committee 440. Guide for the design and construction of concrete reinforced with FRP bars. ACI440.1R-03, American Concrete Institute, Farmington Hills, MI; 2003. p. 42.
[29] ACI Committee 440. Guide for the design and construction of structural concrete reinforced with FRP bars. ACI440.1R-06, American Concrete Institute, Farmington Hills, MI; 2006. p. 44.
[30] ISIS Canada. Reinforcing concrete structures with fiber reinforced polymers, Design Manual No. 3, ISIS Canada, Winnipeg, Manitoba; 2001.
[31] Comité Euro-International du Béton (CEB). Manual on cracking and deformation, Bulletin d'information, No. 158-E; 1985.
[32] Branson DE. Instantaneous and time-dependent deflections of simple and continuous beams. HPR Rep. No.7, Part 1, Alabama Highway Dept., Bureau of Public roads, Montgomery, AL; 1965.
[33] Comité Euro-International du Béton(CEB). CEB-FIB model for concrete structures, Bulletin 213/214; 1990.
[34] Prakhya GKV, Morley CT. Tension stiffening and moment-curvature relations for reinforced concrete elements. ACI Struct J 1990;87(5):597–605.
[35] Kaklauskas G, Ghaboussi J. Stress–strain relations for cracked tensile concrete from RC beam tests. J Struct Eng 2001;127(1):63–73.
[36] Al-Mahaidi RSH. Nonlinear finite element analysis of reinforced concrete deep members. Report No. 79-1, Department of Structural Engineering, Cornell University; 1978. p. 357.
[37] Cedolin L, Poli SD. Finite element studies of shear-critical R/C beams. J Eng Mech Div 1977;103(3):395–410.
[38] Yuzugullu O, Schnobrich WC. A numerical procedure for the determination of the behavior of a shear wall frame system. ACI Struct J 1973;70(7):474–9.
[39] Tanrikulu AK, Dundar C, Cagatay IH. A computer program for the analysis of reinforced concrete frames with cracked beam elements. Struct Eng Mech 2000;10(5):463–78.

[40] Mahroug MEM, Ashour AF, Lam D. Tests of continuous concrete slabs reinforced with carbon fibre reinforced polymer bars. Compos: Part B 2014;66:348–57.
[41] Mahroug MEM, Ashour AF, Lam D. Experimental response and code modelling continuous concrete slabs reinforced with BFRP bars. Compos Struct 2014;107:664–74.
[42] Rafi MM, Nadjai A. Evaluation of ACI 440 deflection model for fiber-reinforced polymer reinforced concrete beams and suggested modification. ACI Struct J 2009;106(6):762–71.
[43] Mosley CP, Tureyen AK, Frosch RJ. Bond strength of nonmetallic reinforcing bars. ACI Struct J 2008;105(5):634–42.